Spontaneously Sliding Multipole Spin Density Waves in Cold Atoms

G. Labeyrie,[1] J. G. M. Walker,[2] G. R. M. Robb,[2] R. Kaiser,[1] and T. Ackemann[2]
[1]Université Côte d'Azur, CNRS, Institut de Physique de Nice, 06560 Valbonne, France
[2]SUPA and Department of Physics, University of Strathclyde, Glasgow G4 0NG, Scotland, United Kingdom

(Received 26 October 2023; revised 27 February 2024; accepted 11 March 2024; published 5 April 2024)

We report on the observation of spontaneously drifting coupled spin and quadrupolar density waves in the ground state of laser driven Rubidium atoms. These laser-cooled atomic ensembles exhibit spontaneous magnetism via light mediated interactions when submitted to optical feedback by a retroreflecting mirror. Drift direction and chirality of the waves arise from spontaneous symmetry breaking. The observations demonstrate a novel transport process in out-of-equilibrium magnetic systems.

DOI: 10.1103/PhysRevLett.132.143402

Magnetic properties of materials have been under intense scrutiny for decades, including complex and yet not fully understood phenomena as its connection to high-T_c superconductivity [1]. Exotic magnetic properties associated to high-order multipole states (quadrupole and beyond) have also recently attracted some interest in heavy-fermion metals [2–6], not the least due to the connection to unconventional superconductivity. Reference [6] concludes on the possibility of the existence of a quadrupolar density wave (QDW), i.e., a modulation of the quadrupolar ordering on length scales larger than the lattice period, analogs to the better known spin density waves (SDW) for dipolar spin states (e.g., [7]) and charge density waves (CDW) for coupled electron density—lattice modulations (e.g., [8]). These density waves are stationary ground states and hence to be distinguished from spin waves, which are collective moving excitations of spin degrees of freedom, whose transport properties are intensely studied with the development of spintronics [9–11]. Nevertheless, a spatial displacement of CDW and SDW demands zero energy and hence in principle they are free to move in any external perturbation, e.g., in an external field (sliding CDW or SDW, see, e.g., [7,8,12] for reviews). This mechanism was originally proposed by Fröhlich to explain superconductivity [13]. However, in practice SDW and QDW are pinned by inhomogeneities of the material and a finite field is needed for depinning, leading also to excess noise, e.g., [7,8,12]. More recently, the question of spontaneous time dependence and spontaneous motion was controversially discussed in the framework of time crystals and space-time crystals with proposals for perpetual motion in ion rings and structured ring-shaped BECs [14–16] but no-go theorems seem to prevent this for the equilibrium ground states of a wide class of autonomous systems [17–19]. The notion of dissipative time crystals for limit cycles in autonomous driven dissipative many-body systems was recently introduced in [20,21].

Cold atom system have emerged as highly controllable simulators for aspects of magnetism and other condensed matter phenomena and time crystals (see, e.g., [22–25] for reviews). In this Letter, we use a diluted cloud of laser-cooled atoms submitted to optical feedback to generate light-mediated magnetic interactions. In this system, spontaneous spatial magnetic ordering occurs, with both dipole and quadrupole coupling [26–28] depending on the magnitude and direction of an applied magnetic field. We stress that these are not pseudo-spins in synthetic magnetic fields, but real magnetic moments in actual B fields, however, a strong coupling is provided by light-mediated interactions so that spontaneous magnetic ordering can emerge in a system which is neither very dense (condensed matter) or ultracold (quantum degenerate gases). We report here the observation of a spontaneously sliding multipolar density wave comprising coupled SDW and QDW whose velocity is set by the magnetic field strength.

In the 1990s, several groups observed spontaneous pattern formation in hot atomic vapors using a retroreflected laser beam [29,30]. For the experiments performed with an effective spin-1/2 structure, these observations corresponded to stationary magnetic dipole ordering due to Zeeman pumping [30,31]. More recently, we have shown using cold ^{87}Rb gases with a more complex energy level structure (corresponding to the $F = 2 \rightarrow F' = 3$ transition of the $D2$ line) that quadrupole interaction terms can play a role in the observed spontaneous ordering [26,28]. These terms are associated with the $\Delta m_F = 2$ Zeeman ground-state coherence induced by the laser fields, hence the name "ground-state coherence" (GSC) was given to this magnetic phase in which dipolar and quadrupolar degrees of freedom are excited.

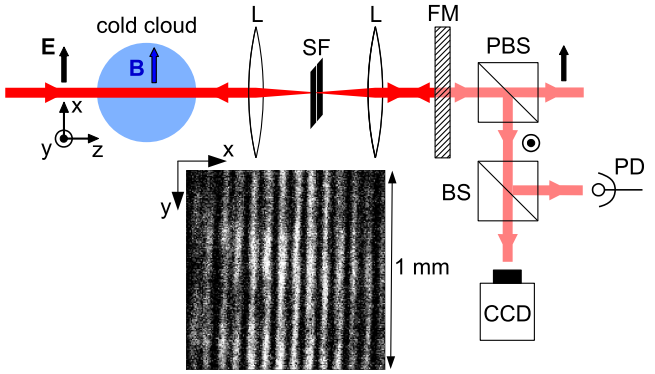

FIG. 1. Experimental scheme. A linearly polarized, red-detuned laser beam is sent through a cloud of cold atoms and retroreflected by a semitransparent feedback mirror (FM). An afocal telescope composed of two lenses (L) allows us to generate an effective FM placed near the rear end of the cloud, inside the vacuum chamber (not shown). A weak magnetic field **B** is applied to the atoms along the direction of the input beam's polarization **E**. A slit (SF) placed inside the telescope allows us to select the transverse wave vectors participating to the optical feedback. The light transmitted by the mirror passes through a polarizing beam splitter (PBS) to select the polarization orthogonal to that of the input beam, and is split in two by a beam splitter (BS). One part is sent to a photodiode (PD) to monitor its temporal fluctuations, while the other is sent onto a CCD. The typical spatial distribution of the light intensity corresponds to stripes, as shown in the inset. Parameters: $I_0 = 4.7$ mW/cm^2, optical density in line center $b_0 = 130$, $\delta = -10\Gamma$, $B_x = 0.14$ G, $\tau_{\text{int}} = 2$ μs. The stripe period is 77.6 μm $= \Lambda_c/2$.

The experimental setup, based on the single feedback mirror (SFM) scheme [32,33], is sketched in Fig. 1 (see also, e.g., Ref. [26]). The nonlinear optical medium is a large, centimeter-sized cloud of cold ^{87}Rb released from a magneto-optical trap. It is illuminated for 1 ms by a 1.8 mm-waist laser beam detuned to the red of the $F = 2 \rightarrow F' = 3$ transition of the $D2$ line by -10Γ, where Γ is the linewidth of the transition. After traversing the cloud the laser beam is retroreflected by a mirror, causing an optical feedback leading to the self-organization of both atomic susceptibility and light intensity in the transverse plane (x, y). The spatial period Λ_c of the emerging structure is determined by the diffractive dephasing between the on-axis pump and the off-axis spontaneously generated sidebands forming the spatial structure [34]. The light intensity distribution in the cross section of the beam is imaged on a camera placed behind the (semitransparent) mirror. A photodiode gives access to the temporal behavior of the transmitted light. All the signals presented here are detected in the linear polarization channel orthogonal to that of the incident light, termed "lin ⊥" hereafter, as a signal in this channel indicates the emergence of the instability on zero background.

The GSC phase is usually composed of several domains with stripes oriented along different directions (see Fig. 3 of Ref. [28], Figs. 12 and 13 of Refs. [34], and [35]). We use a "quasi-1D geometry" (2D in real space, 1D in Fourier space) to facilitate the interpretation of the dynamic measurements. For this, we insert a spatial filter (SF) into the Fourier plane at the middle of an afocal telescope positioned between the cloud and the feedback mirror. In the SFM scheme, the wave number of the patterns is set by the distance between the medium and the feedback mirror due to diffraction, but all transverse wave vectors on a circle with this critical wave number can be excited. Using a simple slit as SF, two opposite wave vectors on this circle are selected. The resulting pattern thus corresponds to stripes oriented perpendicularly to the slit. Here, the stripes are oriented along y, as seen in Fig. 1.

The numerical model used is based on a $F = 1 \rightarrow F' = 2$ transition, simpler than the experimental $F = 2 \rightarrow F' = 3$ to keep the number of coupled equations to solve reasonable, but complex enough to contain the necessary ingredients to explain the observed physics and in particular to allow for the existence of the $\Delta m_F = 2$ ground-state coherence term, $\Phi = 2\rho_{1-1}$. These simulations give access to the time-resolved 2D distributions of atomic and light quantities in the transverse plane. The details of the model can be found in Supplemental Material [26,35].

Figure 2 illustrates the dynamics of the spontaneous magnetic states. In the quasi-1D geometry explained before, drifting stripes can be visualized in the space-time diagrams in Figs. 2(a)–2(d) (see [35] for animations). At a fixed spatial position, both dipole [Fig. 2(d)] and quadrupole [Fig. 2(c)] are periodically oscillating in time. At a fixed time they form a modulated structure in space, consistent with a sliding multipole spin density waves.

For the dipole component, an antiferromagnetic state is connected to a periodic modulation of the longitudinal magnetization $w = \rho_{11} - \rho_{-1-1} = -m_z$ [Fig. 2(d)]. It is given by the difference in occupation ρ_{11} and ρ_{-1-1} in the Zeeman substates of the ground state with positive and negative magnetic quantum numbers. Above a certain pump threshold, this structure emerges spontaneously from the unmodulated optical pump having linear input polarization, i.e., equal amounts of σ_+ and σ_- light (and hence optical spin 0) everywhere and the thermal homogeneous and isotropic atomic cloud. It is sustained by a spontaneously created optical spin structure [Fig. 2(a) shows the σ_+ component, the σ_- lattice is complementary to this]. In turn, this optical spin structure is sustained by spin selective scattering of the pump at the atomic orientation (see [34,35] for details on the mechanism). This antiferromagnetic state constitutes a SDW in the same way as antiferromagnetic ordering in systems with itinerant, i.e., delocalized, electrons [46,47] can be due to SDW (see Supplemental Material Fig. S2 [35] for details). However, this SDW is not stationary but drifts at constant speed. Figures 2(e) and 2(f) illustrate that the total magnetization $\vec{m} = (0, m_y, m_x)$ has a screwlike behavior similar to circularly polarized

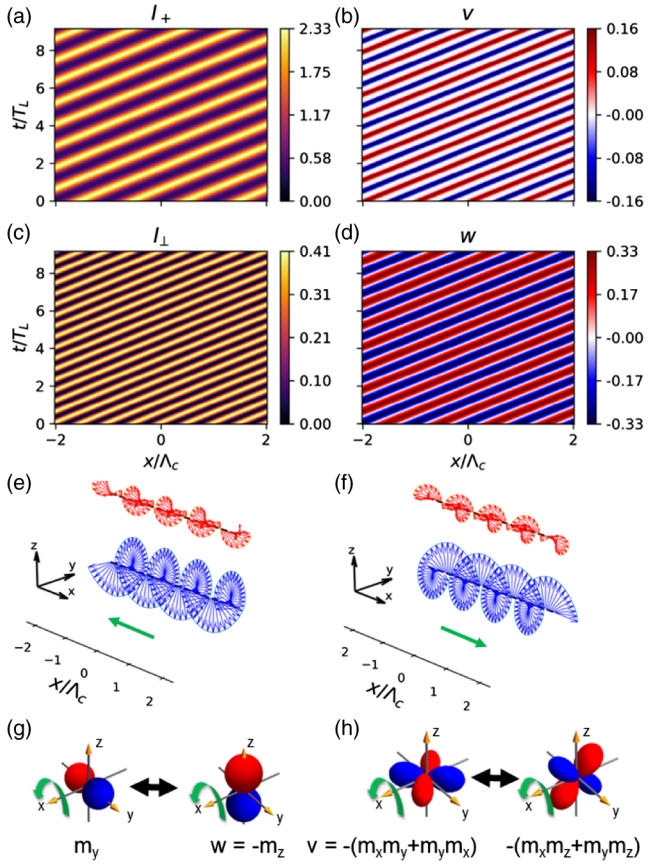

FIG. 2. (a)–(d) Space-time representation of multipolar spin density wave. Space is scaled in units of structure periods, time in units of the Larmor period. Parameters: $B_x = 0.5$ G, $R = 1$, OD $= 70$, $\delta = -10\Gamma_1$, $I_{\text{in}} = 5$ mW/cm^2. (a) Intensity of σ_+ component; (b) intensity of linear polarization component perpendicular to pump corresponding to experimental observable monitored; (c) amplitude of quadrupolar state $v = -(m_x m_z + m_z m_x)$; (d) amplitude of longitudinal orientation $w = -m_z$. (e),(f) Illustration of precession of the magnetization $\vec{m}$ (lower, blue) and of $[0, -(m_x m_y + m_y m_x), -(m_x m_z + m_z m_x)]$ (upper red) representing one of the cones of the quadruple, for $B_x > 0$. The wave in (e) is drifting left in a right-handed screw, the one in (f) right in a left-handed screw. Animations of the full wave dynamics are in [35]. (g),(h) Spherical harmonics illustrating the symmetry of the indicated state multipoles. Red, positive (south pole); blue, negative values (north pole). The direction of precession is indicated by the green arrow.

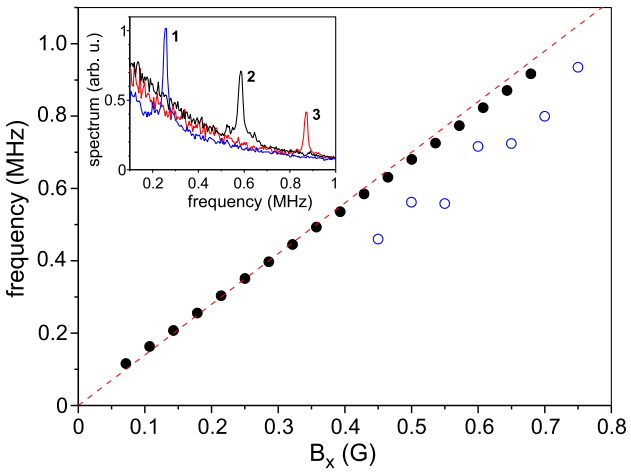

FIG. 3. Temporal dynamics for drifting structures in SMSDW phase. The frequency of the central frequency of the ac peak is plotted as a function of B_x for the parameters in Fig. 1 (black circles). The frequency is obtained from spectra of the diffracted intensity (inset: 1, $B_x = 0.25$ G; 2, $B_x = 0.58$ G; 3, $B_x = 0.87$ G). Results from simulations are denoted by open blue circles with parameters OD $= 130$, $\delta = -10\Gamma_1$, $I_{\text{in}} = 5$ mW/cm^2. The dotted red line indicates two times the Larmor frequency.

light. This is due to the precession in the x-magnetic field [Fig. 2(g)]. We will discuss details on frequencies, speeds, and the spontaneous selection of drift direction and chirality below.

Figure 2(b) illustrates the structure in the quadrupolar component. $v = -2\Im\rho_{-11}$ is the imaginary part of the $\Delta m = 2$ coherence between the stretched states and represents the quadrupole $m_x m_z + m_z m_x = -v$. It vanishes in the homogeneous state but gets excited around 0 in the structured state. The feedback mechanism is linked to the phase sensitivity of the Raman coupling between the stretched states and hence an instability of the phase between the σ_+ and σ_- components (see [34,35]). Its dynamics is locked to the dynamics of the dipole components. Obviously, one cannot represent quadrupoles by a single vector but the trajectory of the tip of one of the quadrupolar cones [red in Figs. 2(e) and 2(f)] can be visualized as $[0, -(m_x m_y + m_y m_x), -(m_x m_z + m_z m_x)]$ [see Fig. 2(h) for the precession of the quadrupole].

The ground states of SDW and CDW have a soft (Goldstone) mode structure and any small perturbation can thus bring this ground state into translational motion. In our experiment, this could be done in a controlled way by a minute tilt of the feedback mirror. However, again like SDW and CDW, these are usually pinned by experimental imperfections and a finite mirror tilt is needed to induce a drift [48]. The striking numerical observation for the multipolar structures in the $J = 1$ ground state is, however, that they *drift spontaneously* even without a mirror tilt, i.e., they represent a spontaneously sliding multipolar spin density wave (SMSDW). We stress that this phenomenon does not occur for the other phases, in particular the antiferromagnetic phase existing around $B \approx 0$ and hexagonal and disordered phases that are observed, when the magnetic field is applied along the laser beam's propagation axis [26,27,49].

w and v as the primary relevant atomic variables oscillate at a frequency close to the Larmor frequency (about 15% smaller, Figs. 2(b) and 2(d); see also Fig. 3). The $\sigma_\pm$-polarization components oscillate at the same frequency [Fig. 2(a)], whereas the linear polarization components

orthogonal to the pump polarization used in the experimental detection scheme oscillates at twice this frequency.

For the verification of the predicted dynamics, we first looked at the temporal fluctuations of the diffracted light detected by the photodiode (see Fig. 1). The Fourier transform of this signal shows a narrow peak whose position is proportional to B_x, as illustrated in Fig. 3. The frequencies observed are slightly lower than twice the Larmor frequency for high enough frequencies (twice, as the observation is done in the perpendicular polarization channel). This matches qualitatively the numerical observations although the observed reduction of frequency is about 15%–27% (compared to only 2%–3% in experiment), which merits further detailed characterization. The shift to lower frequencies is a quite common feature in dynamics with damping.

As camera equipment available to us does not allow a direct visualization of the drift, we recorded a series of forty images with an integration duration τ_{int}, and studied how the contrast of the spatial modulation in these images varied with τ_{int}. From this analysis, we inferred that the stripes do drift, and extracted the drift velocity. Because of the poor signal-to-noise ratio in the images and the fact that for each image the position (phase) of the stripes is different, we used the following procedure to quantify the contrast. We computed the Fourier transform of each image and then averaged the Fourier-transformed images. The amplitude of the peak corresponding to the wave vector of the stripes was taken as our measure of the contrast. Note that this quantity is proportional but not equal to the usual contrast used for interference fringes for instance, and can thus exceed one.

The result of this experiment is shown in Fig. 4(a), for $B_x = 0.14$ G. The dots correspond to the experimental data. The dotted curve shows the expected behavior for a drifting sine wave. The position of each minimum corresponds to a phase drift of $\Delta\varphi = n \times 2\pi$, with n integer. It can be seen that the observed behaviors are qualitatively similar. For the experimental data, the time it takes for the wave to drift by one period is approximately 5.2 μs. This corresponds to a temporal modulation frequency of 0.19 MHz, consistent with the measurement presented in Fig. 3. For a stripe period of 78 μm, the corresponding drift velocity is 15 m/s.

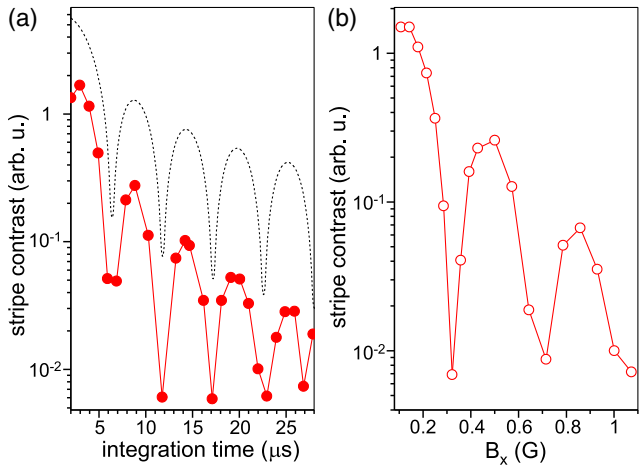

FIG. 4. SMSDW stripe drift. We plot the stripe contrast (see text) versus: (a) camera integration time for $B_x = 0.14$ G; (b) magnetic field B_x for $\tau_{\mathrm{int}} = 2$ μs. Note the vertical logarithmic scale. The dots and circles (+ line to guide the eye) correspond to the experimental data. The dotted curve in (a) is the expectation for a drifting sinusoidal profile.

The impact of the applied magnetic field B_x on the drift velocity is illustrated in Fig. 4(b), where B_x is varied from 0.1 to 1.1 G while the integration time is kept fixed at 2 μs. We observed again a pronounced variation of the contrast, with roughly equidistant minima. As discussed before, the spatial period of the SDW is set by the feedback mirror distance and does not vary with B_x. The observed behavior thus confirms the linear dependence of the drift velocity on B_x. Since the integration time is 2 μs, the modulation frequency corresponding to each minimum in Fig. 4(b) is $n \times 500$ kHz, which is consistent with the data in Fig. 3.

We now return to the discussion of the numerical observations. As observed numerically and experimentally, the diffracted light detected in the orthogonal polarization channel is oscillating at two times the Larmor frequency [compare spacings of stripes in Figs. 2(a) and 2(b)], whereas the fundamental dynamics is at the Larmor frequency. The appearance of the Larmor frequency as the oscillatory time scale is natural. It appears already in models for a $J = 1/2$ ground state [50,51] but was found to be damped for periodic patterns with homogeneous or nearly homogeneous pumping for experimentally accessible parameters. An additional observation from Figs. 2(a) and 2(b) is that w and v are antiphased. This is due to light induced antiphased coupling terms between the dipole and quadrupole components [35]. We conjecture that this additional oscillatory coupling absent in models with a $J = 1/2$ ground state provides the destabilization of the stationary periodic state to a time dependent one, as the simulations indicate that the Larmor oscillations become undamped if the Larmor frequency is of the order of or higher than this coupling frequency. (Note that dipolar and quadrupolar components are not coupled by the magnetic field directly but only via the light mediated coupling.) Interestingly, there is also a strong correlation between antiferromagnetic and quadrupolar ordering in the condensed-matter systems discussed, in particular in Ref. [2].

The drift direction originates from spontaneous symmetry breaking. Starting simulations from noisy initial conditions, the direction of the drift (toward positive or negative x) is found with equal probability for both directions. Interestingly, when we simulate of flip of the direction of B_x during the run, we observe a systematic flip of the drift direction. This can be explained by the direction of precession. Both the magnetization vector $\vec{m} = (0, m_y, m_z)$ and

$[0, -(m_x m_y + m_y m_x), -(m_x m_z + m_z m_x)]$ form a left handed screw in space, if magnetic field and drift direction are parallel to each other, and a right handed screw, if magnetic field and drift direction are antiparallel to each other [Figs. 2(e) and 2(f), details in [35]]. This demonstrates chiral behavior. If the direction of B_x is suddenly flipped, the dynamic state can avoid a reshuffling of the sequence of states by switching the drift direction. This indicates that chirality is the decisive degree of freedom originating from spontaneous symmetry breaking, not drift direction.

Spontaneously drifting structures are also obtained if the Fourier filter is oriented along the y axis, i.e., orthogonal to the applied magnetic field [35]. Here, the plane of precession is not orthogonal to the drift direction x but in the plane spanned by the drift direction and the z axis. Again, spontaneous symmetry breaking leads to chiral behavior corresponding to the situation in the field of chiral quantum optics [52] where the longitudinal polarization component of a strongly nonparaxial light fields and one transverse one couple to elliptically polarized light with the sense of rotation depending on propagation direction.

The observations constitute the demonstration of a novel spontaneous transport process in an out-of-equilibrium magnetic system. From a dynamical point of view, it extends the notion of spontaneous time dependencies in the dissipative time crystals discussed for the superradiant structures in transversely pumped cavities [20,21] from oscillating to drifting states. There is an interesting close phenomenological similarity between the cold atom system discussed here and the condensed matter systems discussed in [2–6], including the strong link between antiferromagnetic ordering (SDW) and quadrupolar ordering (QDW). Even if a direct connection between the condensed-matter Hamiltonians and the cold atom system cannot be established at this stage, the analogy appears to be fruitful, in particular as most experiments in condensed-matter magnetism rely on inferring the structure from macroscopic observables like magnetic susceptibilities and not direct visualization, e.g., [6]. In condensed matter systems, SDW, QDW, and the related CDG for nonmagnetic systems are stationary ground states and drift only after strong enough parity breaking by external fields. The observation of spontaneous drift in a nonequilibrium version of magnetic ordering can be expected to trigger further fruitful research and insight in the question of time crystals and dissipative time crystals in general and spontaneous spin transport in particular.

The collaboration between the two groups is supported by the CNRS-funded Laboratoire International Associé (LIA) "Solace," and the Global Engagement Fund of the University of Strathclyde. We are grateful for useful discussions with Gian-Luca Oppo, Robert Cameron, Benjamin Hourahine, Ivor Kresic, Rina Tazai, and Daniel Hafner.

[1] X. Zhou, W.-S. Lee, M. Imada, N. Trivedi, P. Phillips, H.-Y. Kee, P. Törmä, and M. Eremets, Nat. Rev. Phys. **3**, 462 (2021).
[2] T. Onimaru, T. Sakakibara, N. Aso, H. Yoshizawa, H. S. Suzuki, and T. Takeuchi, Phys. Rev. Lett. **94**, 197201 (2005).
[3] M. Dabrowski, T. R. F. Peixoto, M. Pazgan, A. Winkelmann, M. Cinal, T. Nakagawa, Y. Takagi, T. Yokoyama, F. Bisio, U. Bauer *et al.*, Phys. Rev. Lett. **113**, 067203 (2014).
[4] D. Jang, P. Y. Portnichenko, A. S. Cameron, G. Friemel, A. V. Dukhnenko, N. Y. Shitsevalova, V. B. Filipov, A. Schneidewind, A. Ivanov, D. S. Inosov *et al.*, npj Quantum Mater. **2**, 62 (2017).
[5] R. Tazai and H. Kontani, Phys. Rev. B **100**, 241103(R) (2019).
[6] D. Hafner, P. Khanenko, E.-O. Eljaouhari, R. Küchler, J. Banda, N. Bannor, T. Lühmann, J. F. Landaeta, S. Mishra, I. Sheikin *et al.*, Phys. Rev. X **12**, 011023 (2022).
[7] G. Grüner, Rev. Mod. Phys. **66**, 1 (1994).
[8] G. Grüner, Rev. Mod. Phys. **60**, 1129 (1988).
[9] Y. Kajiwara, K. Harii, S. Takahashi, J. Ohe, K. Uchida, M. Mizuguchi, H. Umezawa, H. Kawai, K. Ando, K. Takanashi *et al.*, Nature (London) **464**, 262 (2010).
[10] I. Žutić, J. Fabian, and S. Das Sarma, Rev. Mod. Phys. **76**, 323 (2004).
[11] A. V. Chumak, V. I. Vasyuchka, A. A. Serga, and B. Hillebrands, Nucl. Phys. **11**, 453 (2015).
[12] S. Cox, J. Singleton, R. D. Mcdonald, A. Migliori, and P. B. Littlewood, Nat. Mater. **7**, 25 (2008).
[13] H. Fröhlich, Proc. R. Soc. A **223**, 296 (1954).
[14] F. Wilczek, Phys. Rev. Lett. **109**, 160401 (2012).
[15] T. Li, Z.-X. Gong, Z.-Q. Yin, H. T. Quan, X. Yin, P. Zhang, L.-M. Duan, and X. Zhang, Phys. Rev. Lett. **109**, 163001 (2012).
[16] F. Robicheaux and K. Niffenegger, Phys. Rev. A **91**, 063618 (2015).
[17] P. Nozières, Europhys. Lett. **103**, 57008 (2013).
[18] P. Bruno, Phys. Rev. Lett. **111**, 070402 (2013).
[19] H. Watanabe and M. Oshikawa, Phys. Rev. Lett. **114**, 251603 (2015).
[20] H. Keßler, P. Kongkhambut, C. Georges, L. Mathey, J. G. Cosme, and A. Hemmerich, Phys. Rev. Lett. **127**, 043602 (2021).
[21] P. Kongkhambut, J. Skulte, L. Mathey, J. G. Cosme, A. Hemmerich, and H. Keßler, Science **377**, 670 (2022).
[22] C. Gross and I. Bloch, Science **357**, 995 (2017).
[23] K. Sacha and J. Zakrzewski, Rep. Prog. Phys. **81**, 016401 (2018).
[24] L. Guo and P. Liang, New J. Phys. **22**, 075003 (2020).
[25] A. J. Daley, I. Bloch, C. Kokail, S. Flannigan, N. Pearson, M. Troyer, and P. Zoller, Nature (London) **607**, 667 (2022).
[26] G. Labeyrie, I. Kresic, G. R. M. Robb, G.-L. Oppo, R. Kaiser, and T. Ackemann, Optica **5**, 1322 (2018).
[27] I. Krešić, G. Labeyrie, G. R. M. Robb, G.-L. Oppo, P. M. Gomes, P. Griffin, R. Kaiser, and T. Ackemann, Commun. Phys. **1**, 33 (2018).
[28] G. Labeyrie, J. G. M. Walker, G. R. M. Robb, R. Kaiser, and T. Ackemann, Phys. Rev. A **105**, 023505 (2022).

[29] G. Grynberg, A. Maître, and A. Petrossian, Phys. Rev. Lett. **72**, 2379 (1994).
[30] T. Ackemann and W. Lange, Phys. Rev. A **50**, R4468 (1994).
[31] A. Aumann, E. Büthe, Y. A. Logvin, T. Ackemann, and W. Lange, Phys. Rev. A **56**, R1709 (1997).
[32] W. J. Firth, J. Mod. Opt. **37**, 151 (1990).
[33] G. D'Alessandro and W. J. Firth, Phys. Rev. Lett. **66**, 2597 (1991).
[34] T. Ackemann, G. Labeyrie, G. Baio, I. Krešić, J. G. M. Walker, A. Costa Boquete, P. Griffin, W. J. Firth, R. Kaiser, G.-L. Oppo *et al.*, Atoms **9**, 35 (2021).
[35] See Supplemental Material at http://link.aps.org/supplemental/10.1103/PhysRevLett.132.143402 for animations and details on theory, which includes Refs. [36–45].
[36] A. Omont, Prog. Quantum Electron. **69**, 5 (1977).
[37] H.-J. Stöckmann and D. Dubbers, New J. Phys. **16**, 053050 (2014).
[38] F. Mitschke, R. Deserno, W. Lange, and J. Mlynek, Phys. Rev. A **33**, 3219 (1986).
[39] J. Dalibard and C. Cohen-Tannoudji, J. Opt. Soc. Am. B **6**, 2023 (1989).
[40] D. A. Steck, Report (2010), available online at http://steck.us/alkalidata (revision 2.1.4, 23 December 2010).
[41] M. Fleischhauer, A. Imamoglu, and J. P. Marangos, Rev. Mod. Phys. **77**, 633 (2005).
[42] G. Labeyrie, E. Tesio, P. M. Gomes, G.-L. Oppo, W. J. Firth, G. R. Robb, A. S. Arnold, R. Kaiser, and T. Ackemann, Nat. Photonics **8**, 321 (2014).
[43] E. Tesio, Ph.D. thesis, Department of Physics, University of Strathclyde, 2014.
[44] S. M. Rochester, Ph.D. thesis, University of California, Berkeley, 2010.
[45] I. Krešić, Ph.D. thesis, Department of Physics, University of Strathclyde, 2017.
[46] J. C. Slater, Phys. Rev. **82**, 538 (1951).
[47] A. W. Overhauser, Phys. Rev. **128**, 1437 (1961).
[48] J. P. Seipenbusch, T. Ackemann, B. Schäpers, B. Berge, and W. Lange, Phys. Rev. A **56**, R4401 (1997).
[49] I. Krešić, G. R. M. Robb, G. Labeyrie, R. Kaiser, and T. Ackemann, Phys. Rev. A **99**, 053851 (2019).
[50] Y. A. Logvin and T. Ackemann, Phys. Rev. E **58**, 1654 (1998).
[51] F. Huneus, B. Schäpers, T. Ackemann, and W. Lange, Appl. Phys. B **76**, 191 (2003).
[52] P. Lodahl, S. Mahmoodian, S. Stobbe, A. Rauschenbeutel, P. Schneeweiss, J. Volz, H. Pichler, and P. Zoller, Nature (London) **541**, 473 (2017).